2025 IEEE/ASME International Conference on Advanced Intelligent Mechatronics (AIM) | 979-8-3315-3342-7/25/$31.00 ©2025 IEEE | DOI: 10.1109/AIM64088.2025.11175812

Hysteresis Modeling and Direct Inverse Compensation Based on Dynamic Time Warping

Zidong Liu[1] and Xu Chen[†,1]

***Abstract*— Actuators based on smart materials often exhibit severe hysteresis nonlinearity. This paper proposes a hysteresis modeling method and a direct inverse model based on the Dynamic Time Warping (DTW) algorithm by analyzing the time-domain characteristics of the input and output signals of actuators with hysteresis. Unlike traditional methods that involve modeling hysteresis loops and solving their inverse models, this study uses DTW to align the input and output signals in the time domain, capturing their temporal discrepancies. An index matrix is introduced to quantify the delay of the output signal relative to the input signal, enabling highly efficient and convenient modeling of hysteresis. The proposed hysteresis model eliminates the need for inverse model computation. Instead, inverse compensation can be achieved simply by using one row of the index matrix obtained during the identification process. Experimental results validate the proposed methods, demonstrating their high accuracy and convenience for modeling asymmetric hysteresis and feedforward compensation.**

***Index Terms*— hysteresis nonlinearity, dynamic time warping, feedforward compensator, motion control**

I. Introduction

Nonlinearity of hysteresis is widely observed in actuators based on smart materials [1]–[3], such as piezoelectric actuators [1], magnetostrictive actuators [2], and shape memory alloys [3]. The hysteresis effect introduces a strong nonlinearity in the input-output relationship of these actuators, significantly degrading their positioning performance. To mitigate the non-linearity of hysteresis, it is typically necessary to first establish a hysteresis model and then derive its corresponding inverse hysteresis model for feedforward compensation [4]. Over many years of development, hysteresis models can be broadly classified into phenomenology-based models, such as the Prandtl-Ishlinskii (PI) model [5], and physics-based models, such as the Jiles-Atherton (JA) model [6]. In precision motion systems such as piezoelectric actuators [7], giant magnetostrictive actuators (GMA) [8], and reluctance actuators [9], phenomenological models are commonly used to describe hysteresis behavior due to their convenience in integrating with control frameworks. The most common phenomenology-based hysteresis models are operator-based models, such as the Preisach model [10], the PI model [5], and their various modifications and extensions [11]–[15]. However, these operator-based hysteresis models typically require solving an inverse model to obtain the inverse hysteresis loop. This inversion process is often cumbersome and imposes a significant computational burden.

The essence of hysteresis lies in the material's physical properties, which cause the output to always lag behind the input in the time domain. Our central finding is that, by a special quantification and recording of this time-domain lag, hysteresis can be effectively modeled. More specifically, we reveal that Dynamic Time Warping (DTW) [16], a dynamic programming algorithm used to measure the similarity between time series, can align two time series and record their alignment order in an index matrix, leading to a new approach of modeling the input and output signals of hysteresis. Furthermore, for an ideal inverse hysteresis model, the inverse hysteresis curve is symmetric to the hysteresis curve about the diagonal line [4]. This means that the degree of input lag relative to output in the hysteresis model is identical to the degree of input lead relative to output in the inverse hysteresis model. We show that this relationship can be fully represented using DTW. Specifically, when DTW aligns two time series A and B, it generates a two-row index matrix, where one row stores the alignment order of A relative to B and the other row stores the alignment order of B relative to A. Thus, DTW enables direct inverse hysteresis modeling without the need to solve the inverse model explicitly, making it highly efficient and convenient for hysteresis compensation.

Figure 1 summarizes the algorithmic realization of the proposed novel framework for hysteresis modeling and inverse compensation, consisting of a DTW-based hysteresis model (DTW-HM) and a DTW-based direct inverse hysteresis model (DTW-DIHM). Compared with conventional approaches, the proposed DTW-HM and DTW-DIHM offer several key advantages. First, they provide high modeling accuracy, with theoretical errors governed by the signal sampling step size – higher sampling rates yield denser data, improving the likelihood of precise mapping. Second, unlike many operator-based models constrained to symmetric hysteresis loops, DTW-HM effectively handles asymmetric hysteresis. Finally, the method enables direct inverse compensation without requiring an explicit solution for the inverse model, making it highly efficient and convenient.

The main contributions of this paper are as follows: 1) We analyze the time-domain behavior of hysteresis loops and reveal that the output signal consistently lags the input with a nearly periodic delay, and that the lag magnitude remains similar across different input amplitudes at a fixed frequency. 2) Leveraging these time-domain characteristics, we propose a novel DTW-based hysteresis model along with a direct inverse compensation method, both of which offer high modeling accuracy and are straightforward to implement. 3)

[†]: corresponding author.

[1]Zidong Liu and Xu Chen are with the Department of Mechanical Engineering, University of Washington, Seattle, WA, USA. {liuzd,chx}@uw.edu

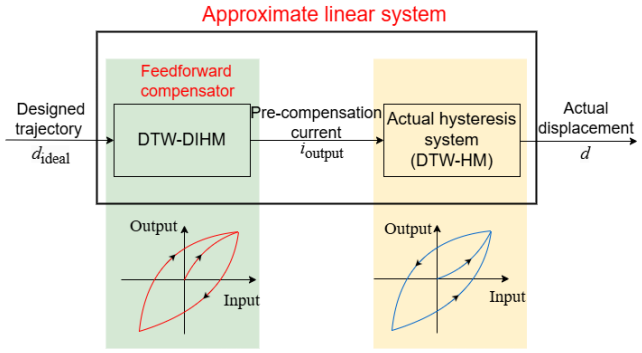

Fig. 1: DTW-HM and DTW-DIHM.

The proposed methods are validated through experiments on a GMA system, demonstrating their effectiveness and showcasing their potential for practical engineering applications.

II. Preliminaries

A. Dynamic Time Warping

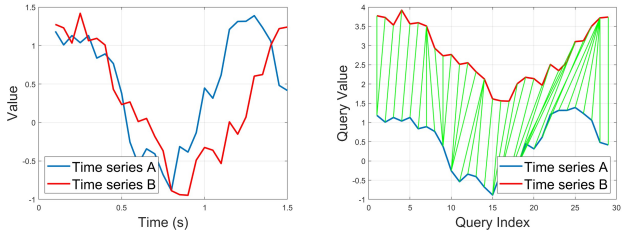

(a) (b)

Fig. 2: An example of dynamic time warping involving two time series datasets in (a), and the minimum Euclidean distance between aligned time series over all permissible temporal alignments in (b).

Consider two time series $A = \{a_1, a_2, \cdots, a_n\}$ and $B = \{b_1, b_2, \cdots, b_m\}$ of lengths n and m, respectively. DTW aligns time series with temporal distortions by identifying an optimal warping path using dynamic programming, as shown in Fig. 2. DTW computes and stores the distance between any two points in the time series in the distance matrix $D_{n\times m}$, as shown in Fig. 3, where each element of the distance matrix is defined as

$$D(i,j) = ||a_i - b_j||_w, \tag{1}$$

where a_i and b_j represent the i-th element and j-th element of A and B, respectively. Subscript w specifies the norm used (e.g. $w = 2$ for the Euclidean distance).

To compute the DTW distance between A and B, an optimal warping path P_{best} should be determined. The warping path is defined as

$$P_{\text{best}} = \{p_1, p_2, \cdots, p_K\}, \tag{2}$$

where K satisfies $\max(n,m) \le K \le n + m - 1$. Each element p_k in the warping path corresponds to an element in the distance matrix $D_{n\times m}$, that is, $p_k = (i,j)_k$, representing the alignment between a_i and b_j. The cost of each alignment is denoted as $D(p_k) = D(i,j)_k$.

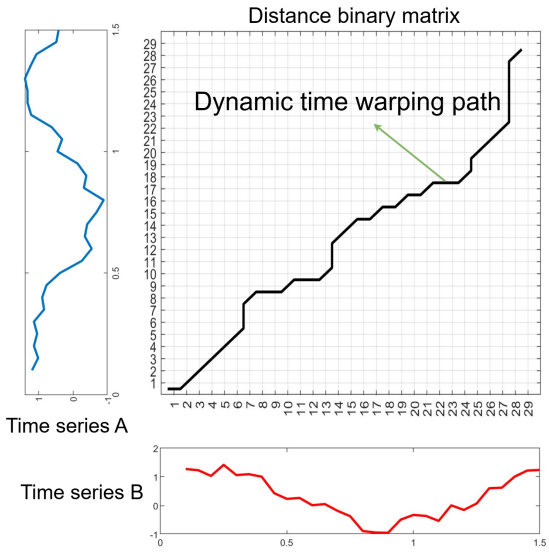

Fig. 3: The process of dynamic time warping.

The warping path must satisfy the following conditions:

- **Boundary condition**: The path starts at the first element of both time series, $p_1 = (1,1)$, and ends at the last element, $p_K = (n,m)$.
- **Monotonicity**: if $p_k = (i,j)$ and $p_{k+1} = (i',j')$, then $i' \ge i$ and $j' \ge j$.
- **Continuity**: if $p_k = (i,j)$ and $p_{k+1} = (i',j')$, then $i' \le i+1$ and $j' \le j+1$, ensuring that all points in each time series are used sequentially.

Among all valid warping paths, the optimal warping path minimizes the cumulative distance, defined as

$$DTW(A,B) = \min\left\{\sum_{k=1}^{K} D(p_k)\right\}. \tag{3}$$

To compute (3), dynamic programming is used to construct a cumulative cost matrix γ, where each element is defined as

$$\gamma(i,j) = D(i,j) + \min\begin{cases}\gamma(i-1,j-1),\\ \gamma(i-1,j),\\ \gamma(i,j-1),\end{cases} \tag{4}$$

where $i = 1,2,\cdots,n$, $j = 1,2,\cdots,m$. The initial conditions are $\gamma(0,0) = 0$, $\gamma(i,0) = \gamma(0,j) = \infty$. Here, $\gamma(i,j)$ represents the cumulative distance at position (i,j), calculated as the sum of $D(i,j)$ and the minimum cumulative distance of its neighboring elements. Thus, $\gamma(n,m)$ represents the minimum cumulative cost between the time series A and B, and $DTW(A,B) = \gamma(n,m)$. To reconstruct the optimal warping path, a backtracking is performed starting from p_K and moving in reverse through the cost matrix, as illustrated in Fig. 3. The process ends when $i = j = 1$ and $p_k(i,j) = (1,1)$, yielding the complete warping path.

B. Hysteresis in the Time Domain

Hysteresis is often represented and studied using the format shown in Fig. 4a, which illustrates the actual hysteresis characteristic and its ideal input-output linear relationship. The particular data here is between the input current i and output displacement d for a GMA system. The slope k between the displacement d and the current i can be obtained by calculating

$$k = \frac{\max(d) - \min(d)}{\max(i) - \min(i)}. \tag{5}$$

Subsequently, we can derive a normalized displacement d_n by

$$d_n = \frac{d}{k}, \tag{6}$$

which has the same amplitude range as the current i. By plotting the current i and the normalized displacement d_n over time, as shown in Fig. 4b, it becomes more intuitive to observe the hysteresis characteristic between the input and output. Moreover, the ideal linear input-output relationship requires the normalized displacement d_n to overlap with the current i. This aligns well with the purpose of DTW, which excels at mapping one time series onto another through optimal alignment paths.

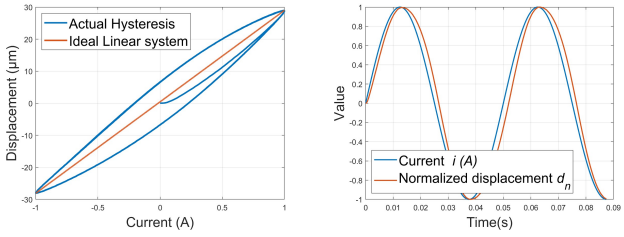

(a) (b)

Fig. 4: Example hysteresis loop and hysteresis in the time domain: (a) actual hysteresis and ideal linear input-output mapping; (b) hysteresis in the time domain.

Fig. 5 illustrates the hysteresis loops between the output displacement and the sinusoidal current input of the GMA at 20 Hz. We define the relative width of the loop as

$$h_{\text{width}} = \frac{h_{\max}}{|\max(d) - \min(d)|} \times 100\%, \tag{7}$$

where $h_{\max}$ represents the difference between the two displacement values in the widest part of the hysteresis loop in Fig. 4a. The higher the value of h_{width}, the rounder the hysteresis loop, indicating a higher degree of output delay relative to the input in the time domain. In contrast, the smaller the value of h_{width}, the closer the hysteresis loop to linearity and the smaller the degree of lag in output relative to input. It can be observed that, at the same frequency, the relative loop width h_{width} for sinusoidal inputs of different amplitudes shows little difference. This indicates that the degree of lag at the same frequency remains consistent. This consistency plays a crucial role in simplifying the identification process of hysteresis models.

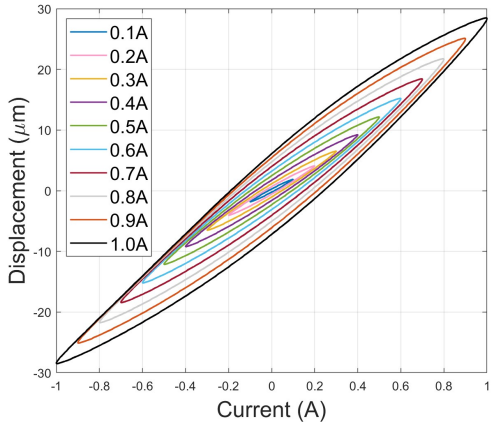

Fig. 5: Hysteresis of the GMA under sinusoidal current inputs of varying amplitudes at 20 Hz.

III. Proposed Hysteresis Modeling and Direct Inverse Compensation Based on Dynamic Time Warping

A. Hysteresis Modeling Based on Dynamic Time Warping

1) Obtaining input-output data from actuators with hysteresis: To achieve the optimal mapping relationship between the input and output of the hysteresis effect, it is necessary first to measure a set of input-output data for identification purposes. This data is used in the DTW to derive the optimal warping path P_{best} described in (2).

2) Displacement normalization: To effectively use DTW, we normalize the displacement d (output data) according to (5) and (6). This normalization process scales the displacement data proportionally to match the range of the current i (input data). The normalized displacement d_n is then obtained, and its lag relative to the current i in the time domain can be illustrated using Fig. 4b.

3) Dynamic time warping (identification process): To accurately fit the hysteresis relationship, DTW is performed between the current i and d_n to obtain the distance matrix $D_{n\times m}$ and the optimal DTW path P_{best}, as shown in Fig. 3.

A two-row index matrix $P_{2\times K}$ is defined for P_{best}, with rows representing the index mappings of time series A (current i) and B (d_n), respectively. As shown in Fig. 3, in the DTW path, diagonal and vertical steps advance the index of A, while horizontal steps repeat it; conversely, diagonal and horizontal steps advance B, while vertical steps repeat it. For the hysteresis shown in Fig. 4b, to fit the hysteresis and obtain the hysteresis model, i and d_n are aligned via DTW. Duplicate indices in the second row of $P_{2\times K}$ are removed, keeping the first occurrence. Corresponding entries in the first row are also removed to yield $P_{2\times K1}$. Finally, a new current trajectory i_{dtw} is generated by reordering i according to the first row of $P_{2\times K1}$, aligning it with d_n as shown in Fig. 6a.

4) Inverse normalization of displacement: By multiplying i_{dtw} with the slope k from (5), the hysteresis model output H_{dtw} is obtained, as shown in Fig. 6b. From Fig. 5, the

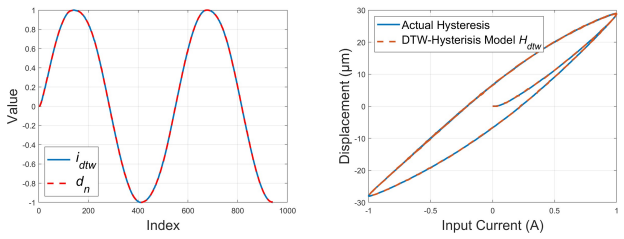

(a) (b)

Fig. 6: DTW hysteresis mapping in the time domain and DTW hysteresis modeling. (a) DTW hysteresis mapping in the time domain. (b) DTW hysteresis modeling.

relative width h_{width} of the hysteresis loops remains nearly constant across different amplitudes at the same frequency, indicating consistent lag behavior. Therefore, for sinusoidal signals at the same frequency, DTW needs to be performed only once to obtain the index matrix $P_{2\times K}$. This matrix can then be reused across amplitudes by scaling the output with the corresponding slope k, enabling accurate modeling while minimizing repeated identification.

B. Direct Inverse Compensation Based on Dynamic Time Warping

The main goal of hysteresis modeling is to enable effective compensation for nonlinearities. Unlike traditional models that require solving inverse operators, the DTW-based method directly yields an inverse model. As shown in Fig. 1, the proposed DTW-DIHM takes the designed trajectory d_{ideal} as the input, and outputs the pre-compensation current i_{output}, which, when applied to the physical system, produces the desired displacement d. This inverse model is constructed by swapping the axes of the *current-normalized displacement* curve, effectively mirroring the hysteresis loop across the diagonal, as illustrated in Fig. 7.

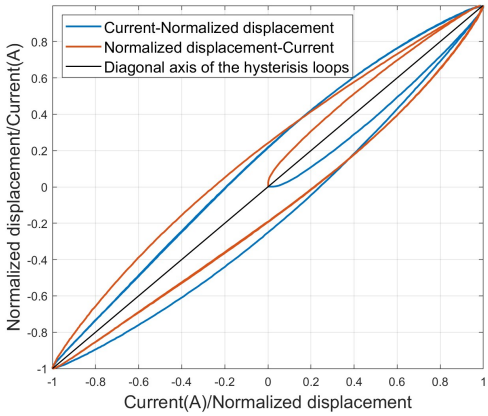

Fig. 7: Illustration of the hysteresis loop and the inverse hysteresis loop.

The direct inverse model can be efficiently constructed using the DTW algorithm. After DTW is applied to an initial set of experimental data, the resulting index matrix $P_{2\times K}$ can be reused to map the normalized ideal displacement $d_{\text{n\_ideal}}$ to a leading pre-compensation current i_{output}. The key principle is that i_{output} should lead $d_{\text{n\_ideal}}$ by the same degree that d_n lags behind the current i in the hysteresis model. This inverse mapping and output sequence are directly obtained using the existing $P_{2\times K}$. More specifically, we have

1) Hysteresis modeling based on DTW: First, the index matrix $P_{2\times K}$ should be obtained following the DTW hysteresis modeling process.

2) Normalization of the ideal displacement trajectory: The ideal displacement trajectory, which represents the target tracking trajectory, is normalized according to (6) to obtain the normalized ideal trajectory $d_{\text{n\_ideal}}$.

3) Output the current according to the index matrix: The direct inverse model of hysteresis corresponds to the mirrored current-normalized displacement relationship, as shown in Fig. 7. It is also evident that the required pre-compensation current i_{output} leads the normalized ideal displacement $d_{\text{n\_ideal}}$ to the same degree that the normalized displacement d_n lags behind the current i during the identification process at the same frequency. The normalized ideal displacement $d_{\text{n\_ideal}}$ and the required pre-compensation current i_{output} are shown in the time domain in Fig. 8a.

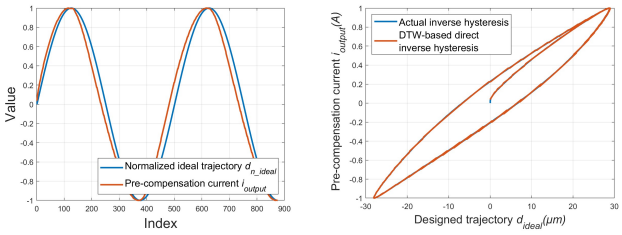

(a) (b)

Fig. 8: Inverse hysteresis and DTW-based direct inverse hysteresis model. (a) Inverse hysteresis in the time domain. (b) DTW-based direct inverse hysteresis model.

For the inverse hysteresis model used in feedforward control, the identification index matrix $P_{2\times K}$ is used to map a standard sinusoidal signal (normalized ideal displacement $d_{\text{n\_ideal}}$) to a signal that leads in the time domain (pre-compensation current i_{output}. However, unlike the previous use of the index matrix $P_{2\times K}$, in this case, time series A (the second row of $P_{2\times K}$) represents the pre-compensation current i_{output}, and time series B represents the normalized ideal trajectory $d_{\text{n\_ideal}}$.

After removing duplicate indices, the resulting refined index matrix $P_{2\times K2}$ allows generation of the pre-compensation current i_{output} that closely aligns with the normalized ideal trajectory, as shown in Fig. 8b.

IV. Experiments and Results

A. Experimental Setup

We utilized a GMA system with significant hysteresis effects as the experimental setup, as illustrated in Fig. 5.

To evaluate the performance of DTW-based hysteresis modeling, we applied sinusoidal current signals of two different amplitudes at a fixed frequency (20 Hz) as inputs: $i_1(t) = 0.5 \times \sin(20 \cdot 2\pi \cdot t)$ (A), $i_2(t) = 0.8 \times \sin(20 \cdot 2\pi \cdot t)$ (A). The results were compared with the PI model to validate the effectiveness of DTW-HM.

To test the feedforward hysteresis compensation capability of DTW-DIHM, two sinusoidal trajectories with different amplitudes at a fixed frequency (20 Hz) were designed as input to the DTW-DIHM: $x_1(t) = 20 \times \sin(20 \cdot 2\pi \cdot t)$ (μm), $x_2(t) = 25 \times \sin(20 \cdot 2\pi \cdot t)$ (μm). The results were compared with the PI inverse hysteresis model (PH-IHM) to assess the performance of the hysteresis compensation.

The index matrix $P_{2\times K}$ used in both experiments was derived from a hysteresis loop, where the input was the first 1.75 cycles of a sinusoidal current signal $i = 0.7 \times \sin(20 \cdot 2\pi \cdot t)$ (A), totaling 875 samples at a 10 kHz sampling rate, and the output was the corresponding measured displacement. The DTW alignment was performed using the Euclidean distance as the similarity metric and a symmetric step pattern. In addition, root mean square error (RMSE: $\sqrt{\frac{1}{T}\sum_{k=1}^{T}|e(t)|^2}$) and maximum absolute error (MAE: $\max|e(t)|$) were used as evaluation metrics to quantify the performance of hysteresis modeling and inverse compensation.

B. Experimental Results & Analysis of Hysteresis Modeling

Fig. 9 and Fig. 10 show the hysteresis modeling results and errors for two different input currents. The related performance evaluation metrics (from 0 to 0.875 s) are recorded in Table I.

For the i_1 signal, as shown in Fig. 9a, the PI hysteresis model demonstrates significant limitations in prediction accuracy, especially at the peak amplitude. In contrast, DTW-HM exhibits much higher accuracy in predicting hysteresis for this signal, which is further confirmed in Fig. 9b. Furthermore, as presented in Table I, the RMSE of the DTW hysteresis model is slightly more than half that of the PI hysteresis model, and its MAE is also smaller. These results indicate that DTW-HM has a significant advantage over the PI model in predicting the hysteresis behavior.

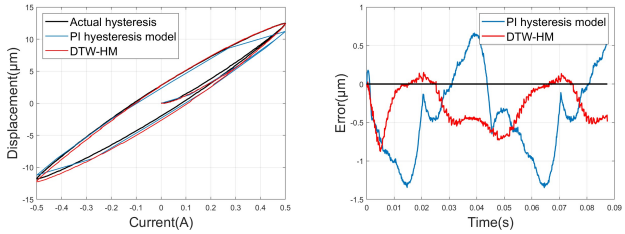

(a) (b)

Fig. 9: Hysteresis loops and corresponding errors under a 0.5A, 20Hz input current: (a) hysteresis loops, (b) modeling errors.

For the i_2 signal, it is evident from Fig. 10a that the prediction results of DTW-HM align more closely with the actual hysteresis data compared to the PI model. This is particularly noticeable during the first 0.25 cycle of the sinusoidal current signal, where the hysteresis behavior differs slightly from that in subsequent cycles, showing a weaker lag. For the PI hysteresis model, which relies on fixed operators, this poses challenges in accurately capturing the hysteresis behavior. In contrast, the DTW-HM offers significant advantages due to its flexibility. It can simultaneously perform dynamic time warping for the first 0.25 cycles and the subsequent cycles. This demonstrates the clear advantage of DTW-HM in capturing the unique hysteresis characteristics of the initial phase and maintaining a high prediction accuracy.

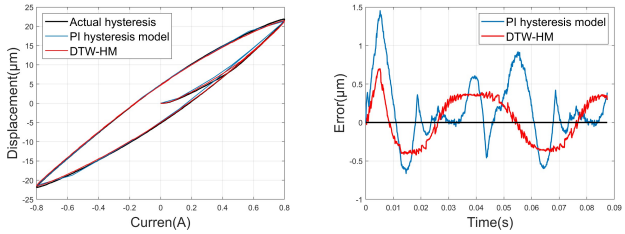

(a) (b)

Fig. 10: Hysteresis loops and corresponding errors under a 0.8A, 20Hz input current: (a) hysteresis loops, (b) modeling errors.

TABLE I: Performance measures of hysteresis modeling

Input current	Model	RMSE (μm)	MAE (μm)
i_1	PI	0.682	1.347
	DTW-HM	**0.384**	**0.876**
i_2	PI	0.447	1.453
	DTW-HM	**0.301**	**0.697**

C. Experimental Results & Analysis of Hysteresis Inverse Compensation

For the two different sinusoidal displacement trajectories, the corresponding hysteresis compensation results and errors are shown in Fig. 11 and Fig. 12, respectively. The related performance evaluation metrics (from 0 to 0.875 s) are summarized in Table II.

For the x_1 trajectory, as shown in Fig. 11a, DTW-DIHM demonstrates better compensation accuracy than PI-IHM, especially at peak positions. As observed in Fig. 11b, its input-output relationship follows the 45° line more closely, indicating a higher linearity. In contrast, the inverse PI model exhibits noticeable deviations, mainly due to less accurate slope estimation during identification. Table II further confirms this, with DTW-DIHM showing significantly lower RMSE and more consistent compensation performance.

For the x_2 trajectory, DTW-DIHM demonstrates a more significant advantage over PI-HIM. As shown in Fig. 12a, PI-HIM exhibits noticeably larger deviations at the initial time compared to DTW-DIHM. From Fig. 12b, it is evident that the compensation results of DTW-DIHM almost perfectly

TABLE II: Performance measures of hysteresis inverse compensation

Designed trajectory	Inverse model	RMSE (μm)	MAE (μm)
x_1	PI-HIM	0.788	1.522
	DTW-DIHM	**0.294**	**1.297**
x_2	PI-HIM	0.471	1.762
	DTW-DIHM	**0.169**	**0.942**

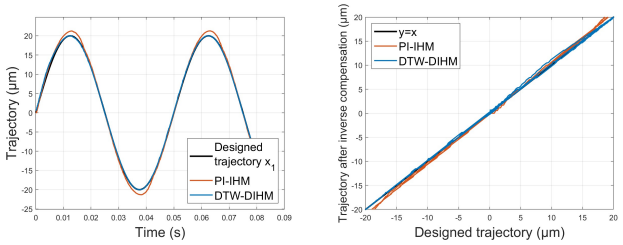

(a) (b)

Fig. 11: Inverse compensation trajectories and effects for the designed trajectory x_1. (a) Inverse compensation trajectories. (b) Inverse compensation effects.

overlap with the 45 ° line, whereas PI-HIM shows significant deviations when the amplitude exceeds zero. Furthermore, as indicated in Table II, the RMSE of DTW-DIHM is only 0.169 μm, which is substantially lower than the 0.471 μm of PI-HIM. Similarly, the MAE of DTW-DIHM is also much smaller than that of PI-HIM. These results highlight the absolute advantages of DTW-DIHM in terms of compensation accuracy and linearity.

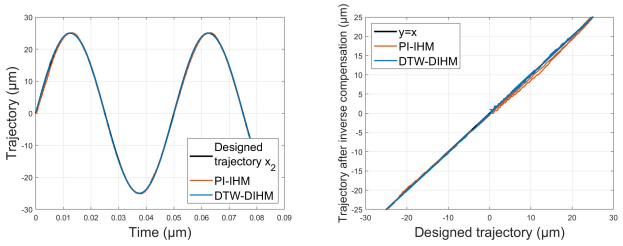

(a) (b)

Fig. 12: Inverse compensation trajectories and effects for the designed trajectory x_2: (a) inverse compensation trajectories, (b) inverse compensation effects.

V. Conclusion

This paper proposes the DTW-HM and DTW-DIHM methods for hysteresis modeling and feedforward compensation in actuators with hysteresis effects. We have analyzed the delay characteristics of hysteresis in the time domain and applied the concept of DTW for time series alignment to the modeling and compensation of hysteresis. Comparative experiments with the PI hysteresis model and PI-IHM demonstrate that DTW-HM and DTW-DIHM are highly effective and accurate for asymmetric hysteresis modeling and inverse compensation. While the proposed DTW-based approach has been demonstrated using sinusoidal trajectories, its structure is applicable to any periodically repeated or predefined reference signals.

References

[1] S. Kang, H. Wu, Y. Li, X. Yang, and J. Yao, "A fractional-order normalized bouc–wen model for piezoelectric hysteresis nonlinearity," *IEEE/ASME Transactions on Mechatronics*, vol. 27, no. 1, pp. 126–136, 2021.

[2] L. Chen, Y. Zhu, J. Ling, and M. Zhang, "Development and characteristic investigation of a multidimensional discrete magnetostrictive actuator," *IEEE/ASME Transactions on Mechatronics*, vol. 27, no. 4, pp. 2071–2079, 2022.

[3] Y. Yu, C. Zhang, Y. Wang, and M. Zhou, "Neural-network-based iterative learning control for hysteresis in a magnetic shape memory alloy actuator," *IEEE/ASME Transactions on Mechatronics*, vol. 27, no. 2, pp. 928–939, 2021.

[4] Z. Li, J. Shan, and U. Gabbert, "A direct inverse model for hysteresis compensation," *IEEE Transactions on Industrial Electronics*, vol. 68, no. 5, pp. 4173–4181, 2020.

[5] M. Al Janaideh, C.-Y. Su, and S. Rakheja, "Development of the rate-dependent prandtl–ishlinskii model for smart actuators," *Smart Materials and Structures*, vol. 17, no. 3, p. 035026, 2008.

[6] M. Sablik, H. Kwun, G. Burkhardt, and D. Jiles, "Model for the effect of tensile and compressive stress on ferromagnetic hysteresis," *Journal of Applied physics*, vol. 61, no. 8, pp. 3799–3801, 1987.

[7] L. Sun, T. Jiang, and X. Chen, "Adaptive loop shaping for wideband disturbances attenuation in precision information storage systems," *IEEE Transactions on Magnetics*, vol. 53, no. 5, pp. 1–13, 2017.

[8] Z. Liu, W. Liu, P. Wang, Z. Li, Y. Xu, X. Yang, and F. Shu, "High-precision position tracking control of giant magnetostrictive actuators using fractional-order sliding mode control with inverse prandtl-ishlinskii compensator," *International Journal of Precision Engineering and Manufacturing*, vol. 24, no. 3, pp. 379–393, 2023.

[9] Z. Liu, Y. Xu, P. Wang, X. Yang, Z. Li, and F. Shu, "Fractional-order sliding mode control with adaptive neural network for high-precision position control of reluctance actuators," in *IECON 2021–47th Annual Conference of the IEEE Industrial Electronics Society*. IEEE, 2021, pp. 1–6.

[10] I. D. Mayergoyz and G. Friedman, "Generalized preisach model of hysteresis," *IEEE transactions on Magnetics*, vol. 24, no. 1, pp. 212–217, 1988.

[11] P.-B. Nguyen, S.-B. Choi, and B.-K. Song, "A new approach to hysteresis modelling for a piezoelectric actuator using preisach model and recursive method with an application to open-loop position tracking control," *Sensors and Actuators A: Physical*, vol. 270, pp. 136–152, 2018.

[12] Z. Li, J. Shan, and U. Gabbert, "Development of reduced preisach model using discrete empirical interpolation method," *IEEE Transactions on Industrial Electronics*, vol. 65, no. 10, pp. 8072–8079, 2018.

[13] U.-X. Tan, W. T. Latt, C. Y. Shee, C. N. Riviere, and W. T. Ang, "Feedforward controller of ill-conditioned hysteresis using singularity-free prandtl–ishlinskii model," *IEEE/ASME Transactions on Mechatronics*, vol. 14, no. 5, pp. 598–605, 2009.

[14] G.-Y. Gu, C.-X. Li, L.-M. Zhu, and C.-Y. Su, "Modeling and identification of piezoelectric-actuated stages cascading hysteresis nonlinearity with linear dynamics," *IEEE/ASME Transactions on Mechatronics*, vol. 21, no. 3, pp. 1792–1797, 2015.

[15] H. Jiang, H. Ji, J. Qiu, and Y. Chen, "A modified prandtl-ishlinskii model for modeling asymmetric hysteresis of piezoelectric actuators," *IEEE Transactions on Ultrasonics, Ferroelectrics, and Frequency Control*, vol. 57, no. 5, pp. 1200–1210, 2010.

[16] H. Sakoe and S. Chiba, "Dynamic programming algorithm optimization for spoken word recognition," *IEEE transactions on acoustics, speech, and signal processing*, vol. 26, no. 1, pp. 43–49, 1978.